Supplementary Information for

Attributing surface temperature difference between a northern mire and forest to their biophysical properties

Erkka Rinne [1] , Juha-Pekka Tuovinen, Maiju Linkosalmi, Juuso Rainne, Sami Suopajärvi, and Mika Aurela

Climate System Research, Finnish Meteorological Institute
P.O. Box 503, 00101, Helsinki, Finland

Supplementary Text 1 Gap-filling of flux data

Fluxes of sensible heat (H) and water vapour (E) as well as friction velocities (u_*) were gap-filled using regression models on suitable meteorological drivers. Temporal data coverages before and after gap-filling are shown in Supplementary Table 1. The models were based on a gradient boosted decision tree algorithm implemented in the Python package `xgboost`, version 3.0.5 (Python 3.12.11). This algorithm has been found to perform well for gap-filling trace gas [1] as well as sensible and latent heat fluxes [2]. The predictor variables for sensible heat and water vapour flux were net radiation, water vapour mass mixing ratio, precipitation, air temperature, wind speed, SWC (only forest) and WTD (only mire). Additionally, H was used as a predictor for E whenever available. Only wind speed was used for modelling u_*. In addition to the aforementioned meteorological variables, all models included the hour of day and day of year (both encoded as $[\sin x, \cos x]$) as predictors for ensuring model time dependency and seasonality. Possible meteorological driver combinations were evaluated using recursive elimination based on the lowest variable importance with 10-fold cross-validation of the adjusted R^2, but the results indicated that it was best to use all available predictors. Only the best quality fluxes (flag 0) and measured meteorological variables were used in training the models, but the final predictions used gap-filled meteorological drivers.

In the model evaluation phase, optimal hyperparameters for the decision tree regression model were chosen using a random search algorithm with mean squared error as the score, but in the final model training all hyperparameter combinations were tested using grid search. The possible hyperparameter values are given in Supplementary Table 2. In the final model training phase, the data were split into training and test sets in the ratio of 9:1 stratified by the available energy, and the models were trained only using the training set. Final model predictions were calculated as the mean of a 10-member model ensemble, each trained using a full-length sample with replacement from the training data set. Model statistical scores calculated using the test data set show good performance with coefficients of determination above 0.76 for all variables (Supplementary Table 3).

For the periods when no sonic anemometer measurements were available, the sonic temperature (T_{sonic}) was calculated from the supporting temperature and humidity measurements:

$$T_{\mathrm{sonic}} = T_{\mathrm{a}}(1 + 0.51q), \tag{S1}$$

where T_{a} is the real absolute air temperature and q the water vapour mole fraction [3]. Furthermore, atmospheric stability was estimated by calculating the Obukhov length using the gap-filled fluxes. The covariances of vertical velocity (w) against temperature and water vapour mixing ratio were solved from the definitions of eddy flux for sensible heat and water vapour, respectively:

$$H = \rho_{\mathrm{d}} c_{\mathrm{p}} \overline{w'T'_{\mathrm{a}}} \tag{S2}$$

$$E = \rho_{\mathrm{d}} \overline{w's'_{\mathrm{v}}}. \tag{S3}$$

The covariance of vertical velocity and sonic temperature T_{sonic} was then estimated using the SND correction [3]:

$$\overline{w'T'_{\mathrm{sonic}}} = \overline{w'T'_{\mathrm{a}}} + 0.51\overline{w'q'}, \tag{S4}$$

Since $q < s_{\mathrm{v}} \ll 1$, we assumed $\overline{w'q'} \approx \overline{w's'_v}$. The Obukhov length was then calculated from the usual definition

$$L = \frac{u_*^3 T_{\mathrm{sonic}}}{\kappa g \overline{w'T'_{\mathrm{sonic}}}}. \tag{S5}$$

Supplementary Table 1: Flux data temporal coverage (%) of the raw data (including measurement gaps etc.), after quality control (QC, excluding measurement gaps) and after gap-filling (GF)

Flux	Site	Raw data	After QC	After GF
Sensible heat	mire	75	60	98
	forest	82	56	99
Water vapour	mire	75	56	98
	forest	82	43	98
Friction velocity	mire	83	63	100
	forest	82	60	99

Supplementary Table 2: Hyperparameter distributions for the gap-filling algorithm

Hyperparameter	Values
`max_depth`	3, 6, 10, 15
`subsample`	0.5, 0.6, 0.7, 0.8, 0.9
`colsample_bytree`	0.5, 0.6, 0.7, 0.8, 0.9
`min_child_weight`	1, 2, 5, 10
`n_estimators`	100, 250, 500, 750

Supplementary Table 3: Mean errors (modelled minus measured), root mean squared errors and coefficients of determination of the gap-filling models calculated using the test data set

Modelled variable (units)	Site	ME	RMSE	R^2
Sensible heat ($\mathrm{W\,m^{-2}}$)	mire	−0.236	5.61	0.87
	forest	−0.400	19.97	0.94
Water vapour ($\mathrm{mmol\,m^{-2}\,s^{-1}}$)	mire	0.022	0.23	0.87
	forest	0.002	0.33	0.83
Water vapour ($\mathrm{mmol\,m^{-2}\,s^{-1}}$) with sensible heat as a predictor	mire	0.029	0.22	0.90
	forest	−0.002	0.30	0.88
Friction velocity ($\mathrm{cm\,s^{-1}}$)	mire	−0.260	5.66	0.76
	forest	0.032	9.33	0.78

Supplementary Text 2 Partial derivatives of the surface temperature equation

Expanding Eq. (19) of the main text gives

$$\begin{aligned}\Delta T_\mathrm{s} = {} & \frac{\partial T_\mathrm{s}}{\partial \alpha}\Delta\alpha + \frac{\partial T_\mathrm{s}}{\partial S_\mathrm{tot}}\Delta S_\mathrm{tot} + \frac{\partial T_\mathrm{s}}{\partial I}\Delta I + \frac{\partial T_\mathrm{s}}{\partial r_\mathrm{a}}\Delta r_\mathrm{a} + \frac{\partial T_\mathrm{s}}{\partial r_\mathrm{s}}\Delta r_\mathrm{s} \\ & + \frac{\partial^2 T_\mathrm{s}}{\partial r_\mathrm{a}^2}\frac{(\Delta r_\mathrm{a})^2}{2!} + \frac{\partial^2 T_\mathrm{s}}{\partial r_\mathrm{s}^2}\frac{(\Delta r_\mathrm{s})^2}{2!} \\ & + 2\frac{\partial^2 T_\mathrm{s}}{\partial \alpha \partial r_\mathrm{a}}\frac{\Delta\alpha\Delta r_\mathrm{a}}{2!} + 2\frac{\partial^2 T_\mathrm{s}}{\partial \alpha \partial r_\mathrm{s}}\frac{\Delta\alpha\Delta r_\mathrm{s}}{2!} + 2\frac{\partial^2 T_\mathrm{s}}{\partial r_\mathrm{a} \partial r_\mathrm{s}}\frac{\Delta r_\mathrm{a}\Delta r_\mathrm{s}}{2!} \\ & + 2\frac{\partial^2 T_\mathrm{s}}{\partial S_\mathrm{tot} \partial r_\mathrm{a}}\frac{\Delta S_\mathrm{tot}\Delta r_\mathrm{a}}{2!} + 2\frac{\partial^2 T_\mathrm{s}}{\partial S_\mathrm{tot} \partial r_\mathrm{s}}\frac{\Delta S_\mathrm{tot}\Delta r_\mathrm{s}}{2!} + 2\frac{\partial^2 T_\mathrm{s}}{\partial I \partial r_\mathrm{a}}\frac{\Delta I\Delta r_\mathrm{a}}{2!} + 2\frac{\partial^2 T_\mathrm{s}}{\partial I \partial r_\mathrm{s}}\frac{\Delta I\Delta r_\mathrm{s}}{2!} \\ & + \ldots,\end{aligned} \tag{S6}$$

where all the partial derivatives are evaluated using the forest data. The terms that equal zero have been omitted.

Assuming independence of the background air temperature and humidity from LST, the partial derivatives of Eq. (16) of the main text with respect to albedo, total energy storage change, SEB imbalance, aerodynamic resistance and bulk surface resistance are, respectively,

$$\frac{\partial T_\mathrm{s}}{\partial \alpha} = -\frac{\lambda_0}{1+f}S_\downarrow \tag{S7}$$

$$\frac{\partial T_\mathrm{s}}{\partial S_\mathrm{tot}} = \frac{\partial T_\mathrm{s}}{\partial I} = -\frac{\lambda_0}{1+f} \tag{S8}$$

$$\frac{\partial T_\mathrm{s}}{\partial r_\mathrm{a}} = \frac{\lambda_0 L_\mathrm{e}\rho_\mathrm{d}D_\mathrm{a}}{(r_\mathrm{a}+r_\mathrm{s})^2(1+f)} + \frac{\partial T_\mathrm{s}}{\partial f}\frac{\partial f}{\partial r_\mathrm{a}} \tag{S9}$$

$$\frac{\partial T_\mathrm{s}}{\partial r_\mathrm{s}} = \frac{\lambda_0 L_\mathrm{e}\rho_\mathrm{d}D_\mathrm{a}}{(r_\mathrm{a}+r_\mathrm{s})^2(1+f)} + \frac{\partial T_\mathrm{s}}{\partial f}\frac{\partial f}{\partial r_\mathrm{s}}, \tag{S10}$$

and second-order partial derivatives

$$\frac{\partial^2 T_\mathrm{s}}{\partial \alpha^2} = \frac{\partial^2 T_\mathrm{s}}{\partial S_\mathrm{tot}^2} = \frac{\partial^2 T_\mathrm{s}}{\partial I^2} = 0 \tag{S11}$$

$$\frac{\partial^2 T_\mathrm{s}}{\partial r_\mathrm{a}^2} = \frac{\partial^2 T_\mathrm{s}}{\partial f^2}\left(\frac{\partial f}{\partial r_\mathrm{a}}\right)^2 + \frac{\partial T_\mathrm{s}}{\partial f}\frac{\partial^2 f}{\partial r_\mathrm{a}^2} - \frac{2\lambda_0 L_\mathrm{e}\rho_\mathrm{d} D_\mathrm{a}}{(r_\mathrm{a}+r_\mathrm{s})^2(1+f)^2}\frac{\partial f}{\partial r_\mathrm{a}} - \frac{2\lambda_0 L_\mathrm{e}\rho_\mathrm{d} D_\mathrm{a}}{(r_\mathrm{a}+r_\mathrm{s})^3(1+f)} \tag{S12}$$

$$\frac{\partial^2 T_\mathrm{s}}{\partial r_\mathrm{s}^2} = \frac{\partial^2 T_\mathrm{s}}{\partial f^2}\left(\frac{\partial f}{\partial r_\mathrm{s}}\right)^2 + \frac{\partial T_\mathrm{s}}{\partial f}\frac{\partial^2 f}{\partial r_\mathrm{s}^2} - \frac{2\lambda_0 L_\mathrm{e}\rho_\mathrm{d} D_\mathrm{a}}{(r_\mathrm{a}+r_\mathrm{s})^2(1+f)^2}\frac{\partial f}{\partial r_\mathrm{s}} - \frac{2\lambda_0 L_\mathrm{e}\rho_\mathrm{d} D_\mathrm{a}}{(r_\mathrm{a}+r_\mathrm{s})^3(1+f)}, \tag{S13}$$

and mixed derivatives

$$\frac{\partial^2 T_\mathrm{s}}{\partial \alpha \partial S_\mathrm{tot}} = \frac{\partial^2 T_\mathrm{s}}{\partial \alpha \partial I} = \frac{\partial^2 T_\mathrm{s}}{\partial S_\mathrm{tot} \partial I} = 0 \tag{S14}$$

$$\frac{\partial^2 T_\mathrm{s}}{\partial \alpha \partial r_\mathrm{a}} = \frac{\lambda_0 S_\downarrow}{(1+f)^2}\frac{\partial f}{\partial r_\mathrm{a}} \tag{S15}$$

$$\frac{\partial^2 T_\mathrm{s}}{\partial \alpha \partial r_\mathrm{s}} = \frac{\lambda_0 S_\downarrow}{(1+f)^2}\frac{\partial f}{\partial r_\mathrm{s}} \tag{S16}$$

$$\frac{\partial^2 T_\mathrm{s}}{\partial S_\mathrm{tot} \partial r_\mathrm{a}} = \frac{\partial^2 T_\mathrm{s}}{\partial I \partial r_\mathrm{a}} = \frac{\lambda_0}{(1+f)^2}\frac{\partial f}{\partial r_\mathrm{a}} \tag{S17}$$

$$\frac{\partial^2 T_\mathrm{s}}{\partial S_\mathrm{tot} \partial r_\mathrm{s}} = \frac{\partial^2 T_\mathrm{s}}{\partial I \partial r_\mathrm{s}} = \frac{\lambda_0}{(1+f)^2}\frac{\partial f}{\partial r_\mathrm{s}} \tag{S18}$$

$$\frac{\partial^2 T_\mathrm{s}}{\partial r_\mathrm{a} \partial r_\mathrm{s}} = \frac{\partial T_\mathrm{s}}{\partial f}\frac{\partial^2 f}{\partial r_\mathrm{a} \partial r_\mathrm{s}} + \frac{\partial^2 T_\mathrm{s}}{\partial f^2}\frac{\partial f}{\partial r_\mathrm{a}}\frac{\partial f}{\partial r_\mathrm{s}} - \frac{\lambda_0 L_\mathrm{e}\rho_\mathrm{d} D_\mathrm{a}}{(r_\mathrm{a}+r_\mathrm{s})^2(1+f)^2}\left(\frac{\partial f}{\partial r_\mathrm{a}} + \frac{\partial f}{\partial r_\mathrm{s}}\right) - \frac{2\lambda_0 L_\mathrm{e}\rho_\mathrm{d} D_\mathrm{a}}{(r_\mathrm{a}+r_\mathrm{s})^3(1+f)}, \tag{S19}$$

where

$$\frac{\partial T_\mathrm{s}}{\partial f} = -\frac{\lambda_0\left(R_\mathrm{n}^* - S_\mathrm{tot} - I - \frac{L_\mathrm{e}\rho_\mathrm{d} D_\mathrm{a}}{r_\mathrm{a}+r_\mathrm{s}}\right)}{(1+f)^2} \tag{S20}$$

$$\frac{\partial^2 T_\mathrm{s}}{\partial f^2} = \frac{2\lambda_0\left(R_\mathrm{n}^* - S_\mathrm{tot} - I - \frac{L_\mathrm{e}\rho_\mathrm{d} D_\mathrm{a}}{r_\mathrm{a}+r_\mathrm{s}}\right)}{(1+f)^3} \tag{S21}$$

$$\frac{\partial f}{\partial r_\mathrm{a}} = -\lambda_0\rho_\mathrm{d} c_\mathrm{p}\left(\frac{1}{r_\mathrm{a}^2} + \frac{L_\mathrm{e}\Delta_\mathrm{a}^*}{c_\mathrm{p}(r_\mathrm{a}+r_\mathrm{s})^2}\right) \tag{S22}$$

$$\frac{\partial^2 f}{\partial r_\mathrm{a}^2} = 2\lambda_0\rho_\mathrm{d} c_\mathrm{p}\left[\frac{1}{r_\mathrm{a}^3} + \frac{L_\mathrm{e}\Delta_\mathrm{a}^*}{c_\mathrm{p}(r_\mathrm{a}+r_\mathrm{s})^3}\right] \tag{S23}$$

$$\frac{\partial f}{\partial r_\mathrm{s}} = -\frac{\lambda_0 L_\mathrm{e}\rho_\mathrm{d}\Delta_\mathrm{a}^*}{(r_\mathrm{a}+r_\mathrm{s})^2} \tag{S24}$$

$$\frac{\partial^2 f}{\partial r_\mathrm{s}^2} = \frac{\partial^2 f}{\partial r_\mathrm{a} \partial r_\mathrm{s}} = \frac{2\lambda_0 L_\mathrm{e}\rho_\mathrm{d}\Delta_\mathrm{a}^*}{(r_\mathrm{a}+r_\mathrm{s})^3}. \tag{S25}$$

Supplementary Text 3 Model evaluation

The SEB-derived surface temperatures ($T_\mathrm{s}^\mathrm{SEB}$) correlated very well with the corresponding air temperatures measured within the forest canopy and at the ground level in the mire. In the forest, the Pearson correlation between the 30-min $T_\mathrm{s}^\mathrm{SEB}$ and the mean within canopy air temperature was greater than 0.99 with a mean error of $-0.12\,^\circ$C. In

the mire, the correlation between the 30-min $T_\mathrm{s}^\mathrm{SEB}$ and the wind-sector (EC footprint area) averaged near-surface air temperature was 0.93 with a mean error of 0.42 °C. For the daytime and nighttime datasets, the mean error in the mire was larger in magnitude, +1.7 and −1.3 °C, respectively, i.e. during daytime the surface was on average warmer and during nighttime cooler than the air right above it, indicating that the air temperature even very close to the surface (2 cm) could have a delayed response to LST. However, this could also be due to the slowness of the temperature sensors themselves.

With the above comparisons, we could establish that $T_\mathrm{s}^\mathrm{SEB}$ represented the LST reasonably well. The approximations made for the linearised surface temperature equation did not affect the accuracy much: the linearised T_s matched $T_\mathrm{s}^\mathrm{SEB}$ nearly perfectly with Pearson correlations greater than 0.99 and mean absolute errors less than 0.04 °C at both sites.

Comparing the differences in $T_\mathrm{s}^\mathrm{SEB}$ between the sites to the attribution models' ΔT_s showed much more scatter. In Supplementary Figure 1, the attribution models are compared against $T_\mathrm{s}^\mathrm{SEB}$ using different Taylor series reference points and polynomials of degrees 1, 2 and 4.

We quantified the performance of the attribution models Eqs. (19)–(21) against the differences in $T_\mathrm{s}^\mathrm{SEB}$ using the modified Kling–Gupta Efficiency score (mKGE) which takes into account correlation, variability and bias [4]:

$$\mathrm{mKGE} = 1 - \sqrt{(r-1)^2 + (\beta-1)^2 + (\gamma-1)^2}, \tag{S26}$$

where r is the correlation coefficient between modelled and measured values, $\beta = \hat{\mu}/\mu$ the relationship between their means and $\gamma = \frac{\hat{\sigma}/\hat{\mu}}{\sigma/\mu}$ the relationship between their coefficients of variation. An mKGE-value of 1 would be optimal. As the attribution model results contained some unrealistically low or large values of LST difference, we used Spearman's rank correlation, which is more robust to outliers than the Pearson correlation coefficient. As robust estimators for the mean and standard deviation (σ), we used the median and the median absolute deviation (Python function `scipy.stats.median_abs_deviation`, SciPy version 1.16.1), respectively, to reduce the impact of outliers in the data. mKGE was also used to optimise the weight of the partial derivatives in the weighted model (Section 4.5) and the reference point of Eq. (21) using the Python function `scipy.optimize.minimize_scalar`.

The first-degree attribution model about the mean values of the attributed variables (Eq. (21)) performed best in all temporal averaging scales, and increasing the Taylor polynomial degree did not improve the model (Supplementary Table 4). By definition, even-degree terms in Eq. (21) cancel out, and hence the second-degree model is essentially the same as the first-degree model and similarly for the fourth- and third-degree models. On the other hand, increasing the polynomial degree for the attribution models about the attributed variable values in the forest or in the mire (Eq. (19) for the former) improved the models considerably, indicating that the higher degree terms take into account the non-linearities and cross-correlations of the variables when the reference point is far from the other variable state. Using a mean reference point alleviates some of the errors in the low-degree models, which cannot take into account auto- and cross-correlations between the surface properties. The high-degree models suffered from a number of data points (days) where the difference in surface properties, especially r_s, was very large leading to some huge values of $(\Delta r_\mathrm{s})^n$ with $n \geq 2$ (not shown), but this had very little impact on the final results.

The first-degree model utilising both reference points (Eq. (20)) performed better than either of the models with only a single reference point, but increasing the polynomial degree did not improve the attribution accuracy. The weighted model with an optimised coefficient of $m = 0.67$ performed better than the model with equally weighted reference points, but was still outperformed by the mean state model. The optimal reference point between the two states was close to their mean, at $k = 0.48 \pm 0.06$ (mean ± standard error of 100 times bootstrapped estimate), providing evidence for the theoretical optimum of 0.5, which was used for the final analysis.

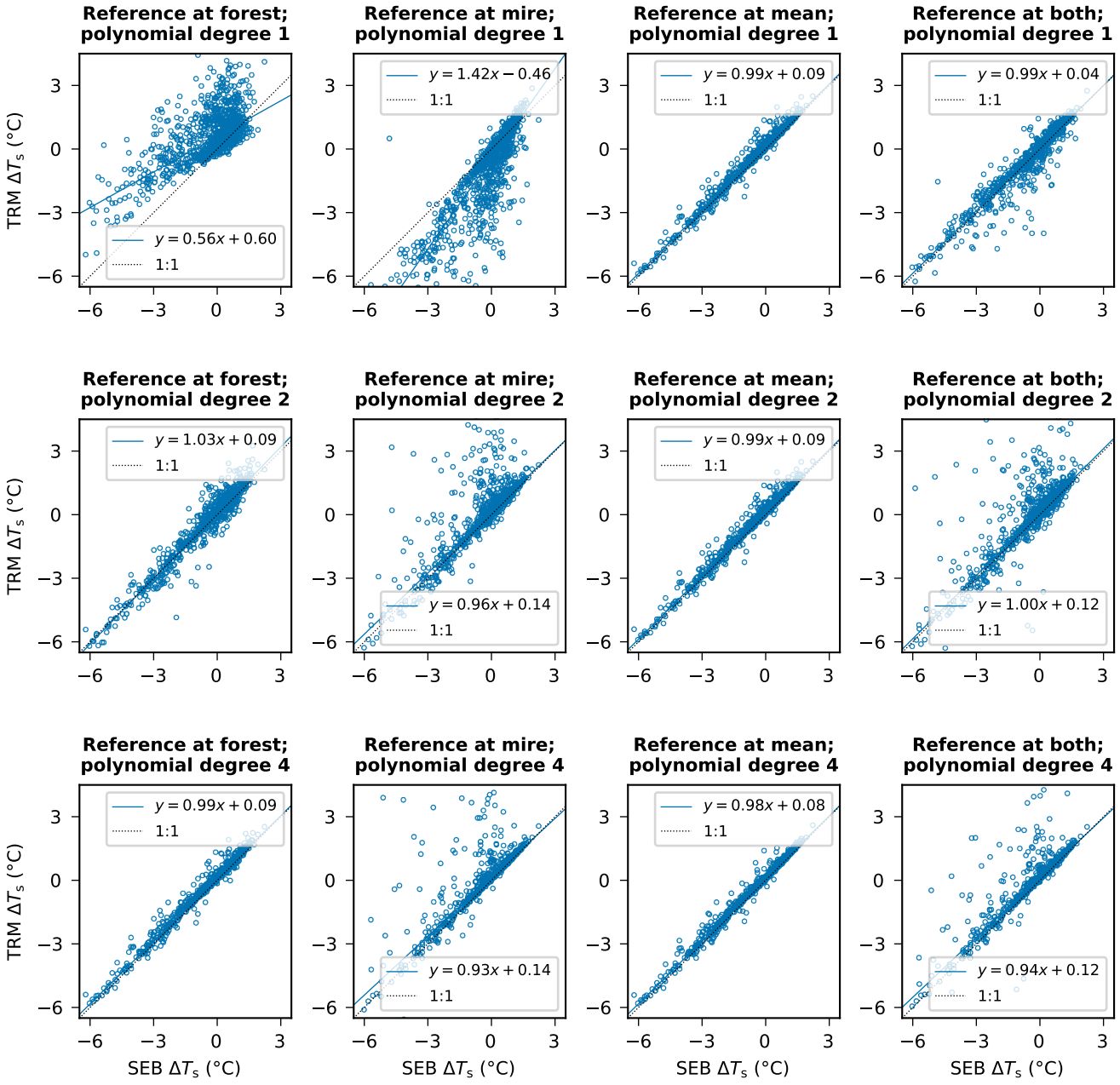

Supplementary Figure 1: Daily mean surface temperature difference calculated with the two-resistance mechanism (TRM) attribution model against the corresponding difference evaluated from the non-linear SEB equation. The comparison is shown for the 1st, 2nd and 4th degree Taylor polynomials. Parameters of robust least-squares linear fits are shown in the legend boxes. The y-axes are limited to a range that excludes large outliers in the modelled temperature difference.

Supplementary Table 4: Modified Kling–Gupta Efficiency of the attribution models with different reference points using Taylor polynomials of varying degree

Reference state	Taylor polynomial degree	Averaging period		
		daily	day	night
forest	1	0.53	0.34	0.66
	2	0.82	0.84	0.81
	3	0.91	0.88	0.88
	4	0.94	0.90	0.92
mire	1	−0.24	−0.22	0.14
	2	0.60	0.79	−0.11
	3	0.53	0.72	−0.30
	4	0.50	0.74	−0.15
both	1	0.75	0.88	0.63
	2	0.68	0.82	0.12
	3	0.67	0.77	0.01
	4	0.57	0.77	−0.06
weighted	1	0.89	0.80	0.76
mean	1	0.95	0.93	0.94
	2	0.95	0.93	0.94
	3	0.91	0.92	0.97
	4	0.91	0.92	0.97

Other supplementary material

Supplementary Table 5: Proportion of different weather situations (%) grouped by seasons

	All data	Winter	Late winter	Spring	Summer	Autumn
Warm	16.3	10.9	18.3	18.0	22.5	17.8
Cold	6.9	9.7	8.7	4.6	3.9	4.1
Dry	14.8	15.6	9.3	15.9	20.4	14.7
Wet	16.5	15.8	16.7	13.4	17.8	18.9
Warm & dry	5.4					
Cold & dry	0.8					
Warm & wet	1.6					
Cold & wet	0.3					

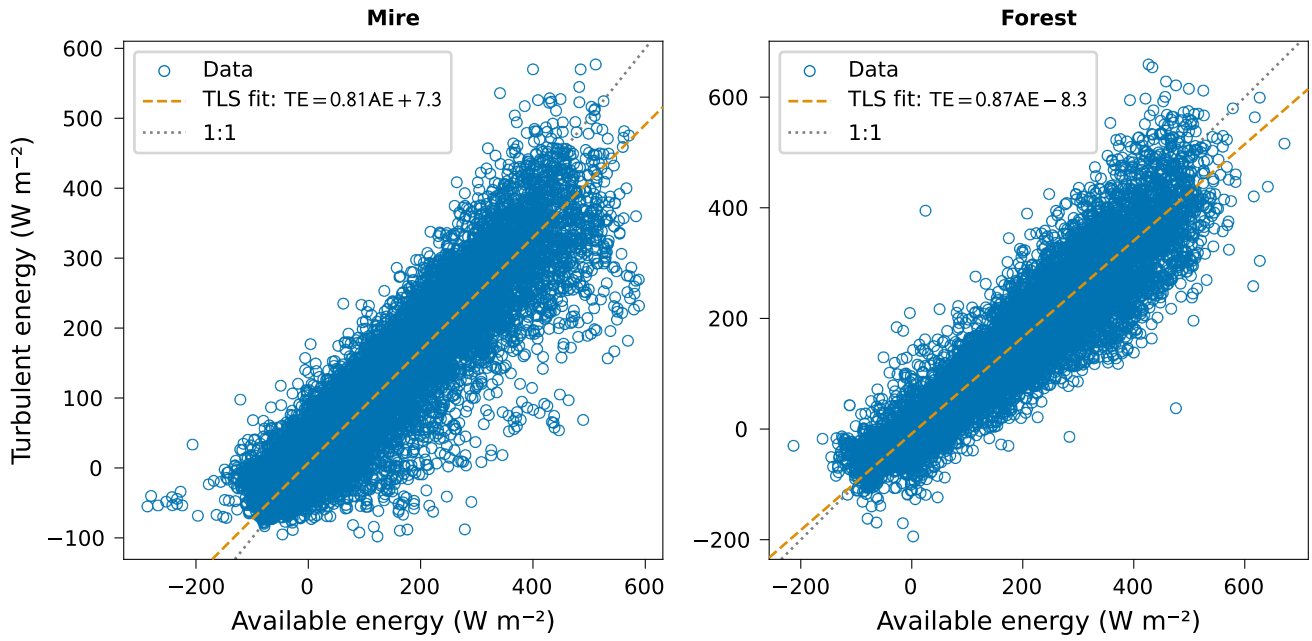

a Uncorrected fluxes

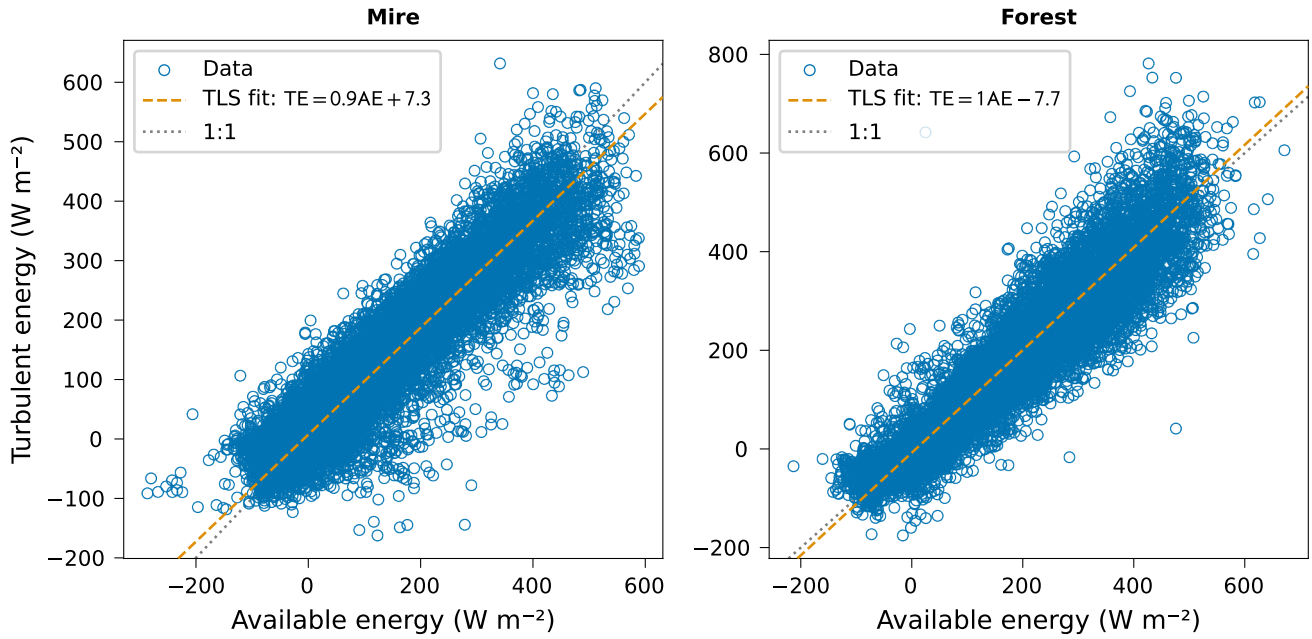

b Corrected fluxes

Supplementary Figure 2: Turbulent energy (TE) versus available energy (AE) for each 30 min period of gapfilled data with uncorrected (a) and corrected turbulent heat fluxes (b). The legend boxes show total least squares fits to the data indicating the energy balance closure as the coefficient of AE.

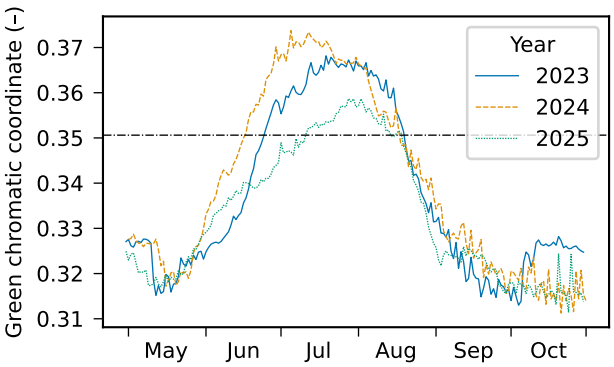

Supplementary Figure 3: Green Chromatic Coordinate (GCC) values calculated from the phenocamera images taken from the mire. The horizontal line indicates the summer threshold at the 67th percentile of all valid GCC values.

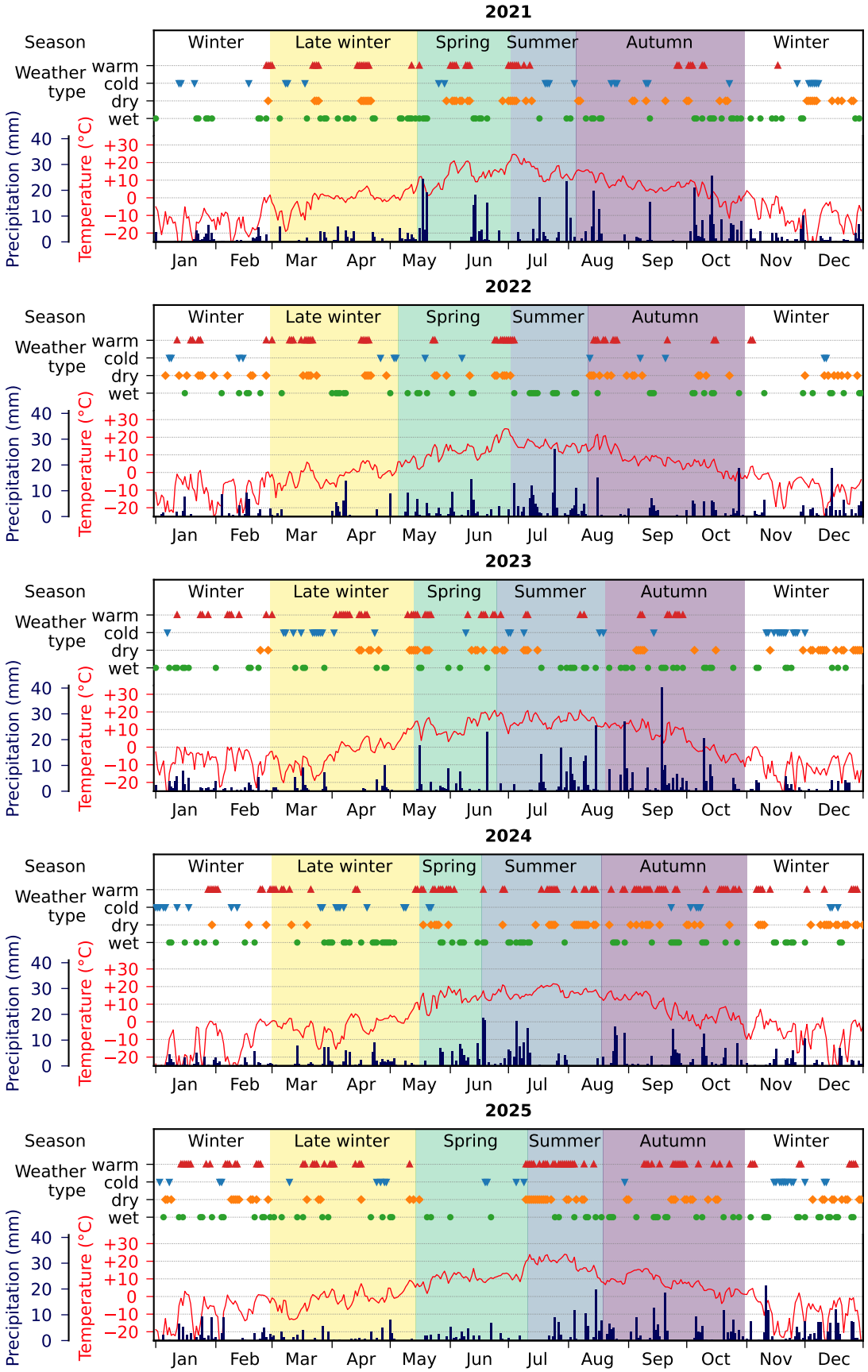

Supplementary Figure 4: Daily mean air temperature (red lines) and daily total precipitation (blue bars) in Sodankylä Tähtelä (WMO 02836). Coloured shadings with names at the top show season classifications based on albedo and the green chromatic index in the mire site. Unshaded (white) areas were not classified to any season. Coloured symbols show weather type classifications for each day.

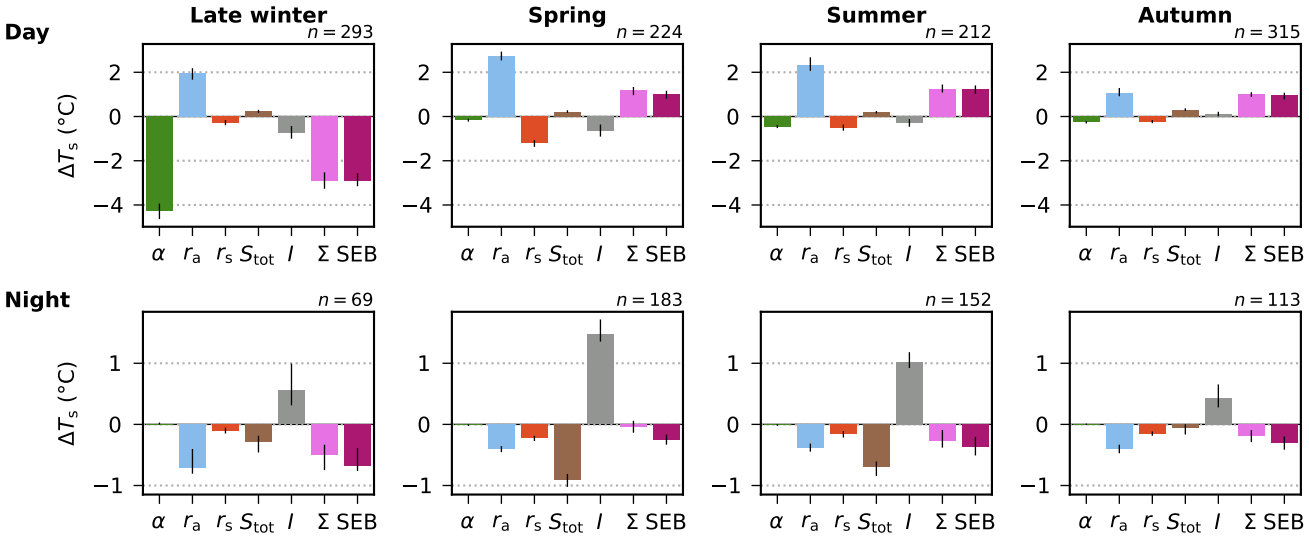

Supplementary Figure 5: Attribution of the difference in mean surface temperature during daytime (top panels) and nighttime (bottom panels) between the mire and the forest to the differences in their biophysical properties (x-axis): albedo (α), aerodynamic resistance (r_a), surface resistance (r_s), total energy storage change (S_{tot}) and SEB imbalance (I). Σ is the sum of the attributed variables, and 'SEB' is the difference in surface temperatures iterated from the parametrised surface energy balance equation. Bar tops indicate median values, and the error bars span their 95 % confidence intervals. The top right corner n shows the number of days in each category. Note the different y-axis scales during day and night.

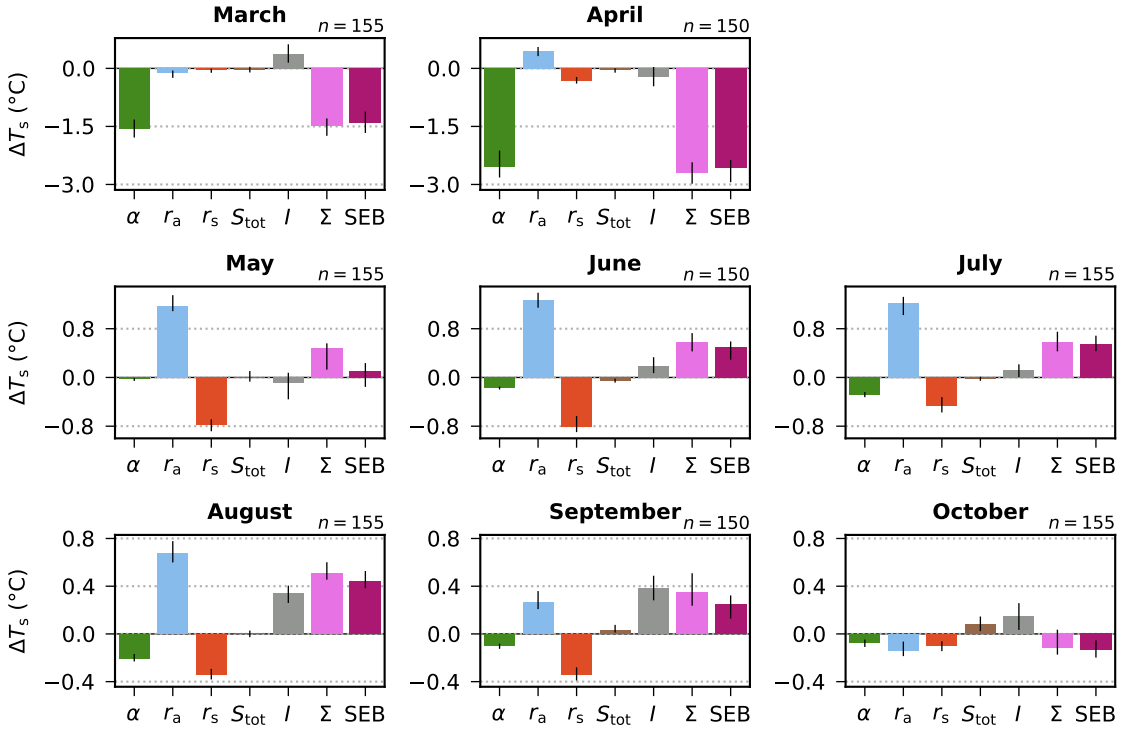

Supplementary Figure 6: Attribution of the difference in daily mean surface temperature between the mire and the forest to the differences in their biophysical properties (x-axis): albedo (α), aerodynamic resistance (r_a), surface resistance (r_s), total energy storage change (S_{tot}) and SEB imbalance (I). Σ is the sum of the attributed variables, and 'SEB' is the difference in surface temperatures iterated from the parametrised surface energy balance equation. Bar tops indicate median values, and the error bars span their 95 % confidence intervals. The top right corner n shows the number of years in each panel. Note the different y-axis scales on different rows.

Supplementary References

1. Vekuri, H. et al. A Widely-Used Eddy Covariance Gap-Filling Method Creates Systematic Bias in Carbon Balance Estimates. *Sci Rep* **13,** 1720 (2023).
2. Rinne, E., Vekuri, H., Aurela, M. & Tuovinen, J.-P. *A Comparison of Methods for Gap-Filling Sensible and Latent Heat Fluxes in Different Climatic Conditions* poster. European Geosciences Union General Assembly 2023, Vienna, Austria. 2023.
3. Schotanus, P., Nieuwstadt, F. & De Bruin, H. Temperature Measurement with a Sonic Anemometer and Its Application to Heat and Moisture Fluxes. *Boundary-Layer Meteorol* **26,** 81–93 (1983).
4. Kling, H., Fuchs, M. & Paulin, M. Runoff Conditions in the Upper Danube Basin under an Ensemble of Climate Change Scenarios. *Journal of Hydrology* **424–425,** 264–277 (2012).